ACS chemical biology

Articles

pubs.acs.org/acschemicalbiology

Chemical Correction of Pre-mRNA Splicing Defects Associated with Sequestration of Muscleblind-like 1 Protein by Expanded r(CAG)-Containing Transcripts

Amit Kumar,[†] Raman Parkesh,[†] Lukasz J. Sznajder,[‡] Jessica L. Childs-Disney,[†] Krzysztof Sobczak,*[,‡] and Matthew D. Disney*[,†]

[†]Department of Chemistry, The Scripps Research Institute, Scripps Florida, 130 Scripps Way 3A1, Jupiter, Florida 33458, United States

[‡]Department of Gene Expression, Institute of Molecular Biology and Biotechnology, Adam Mickiewicz University, Umultowska 89, 61-614 Poznan, Poland

Supporting Information

ABSTRACT: Recently, it was reported that expanded r(CAG) triplet repeats (r(CAG)^{exp}) associated with untreatable neurological diseases cause pre-mRNA mis-splicing likely due to sequestration of muscleblind-like 1 (MBNL1) splicing factor. Bioactive small molecules that bind the 5′CAG/3′GAC motif found in r(CAG)^{exp} hairpin structure were identified by using RNA binding studies and virtual screening/chemical similarity searching. Specifically, a benzylguanidine-containing small molecule was found to improve pre-mRNA alternative splicing of MBNL1-sensitive exons in cells expressing the toxic r(CAG)^{exp}. The compound was identified by first studying the binding of RNA 1×1 nucleotide internal loops to small molecules known to have affinity for nucleic acids. Those studies identified 4′,6-diamidino-2-phenylindole (DAPI) as a specific binder to RNAs with the 5′CAG/3′GAC motif. DAPI was then used as a query molecule in a shape- and chemistry alignment-based virtual screen to identify compounds with improved properties, which identified 4-guanidinophenyl 4-guanidinobenzoate, a small molecule that improves pre-mRNA splicing defects associated with the r(CAG)^{exp}-MBNL1 complex. This compound may facilitate the development of therapeutics to treat diseases caused by r(CAG)^{exp} and could serve as a useful chemical tool to dissect the mechanisms of r(CAG)^{exp} toxicity. The approach used in these studies, defining the small RNA motifs that bind small molecules with known affinity for nucleic acids and then using virtual screening to optimize them for bioactivity, may be generally applicable for designing small molecules that target other RNAs in the human genomic sequence.

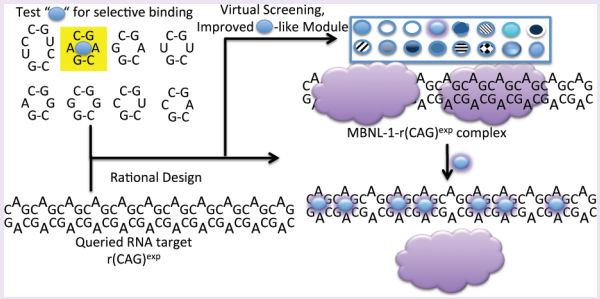

It is known that RNA forms a variety of structures that impart diverse functions.[1,2] For example, RNA catalyzes chemical reactions,[3] riboswitches and microRNAs regulate complex networks of gene expression,[4,5] and RNA encodes and synthesizes protein.[6] Thus, RNA is an important target for chemical genetics probes or therapeutics.[7,8] One advantage of using RNA as a drug target is that structural information can be accurately deduced from sequence. For example, secondary structural information, which includes the motifs that comprise an RNA, can be obtained by free energy minimization[9,10] or phylogenic comparison.[11] Once the ensemble of motifs present in an RNA target are known, modular assembly strategies can be applied to target multiple motifs within a target RNA simultaneously to improve affinity and specificity.[12−14] Most RNAs are underutilized as targets, however, because of a general lack of information that is available on small molecule-RNA interactions.

In order to more effectively design compounds that target RNA, more information is needed on the RNA motifs that can be targeted by small molecules. One class of small molecules that binds to RNA motifs is DNA-binding agents.[15,16] Of particular interest is the binding of these DNA-binding agents to 1×1 nucleotide RNA internal loops because they are present in expanded triplet repeat RNAs that contribute to neurological and neuromuscular disorders such as myotonic dystrophy type 1 (DM1), Huntington's disease (HD), spinocerebellar ataxia type 3 (SCA3), and fragile X-associated tremor-ataxia syndrome (FXTAS). All r(CNG) repeats form similar hairpin architectures; the only difference is the identity of the internal loop nucleotides (U/U, A/A, or G/G internal loops).

Thus, competition dialysis and spectroscopic methods were employed to determine the selectivity of DNA-binding agents to 1×1 nucleotide RNA internal loops (Figure 1) in an effort to identify small molecule leads targeting these structures. Such leads could be further optimized for bioactivity. From these investigations, it was determined that 4′,6-diamidino-2-phenyl-

Received: October 14, 2011
Accepted: December 12, 2011
Published: January 17, 2012

   dx.doi.org/10.1021/cb200413a | ACS Chem. Biol. 2012, 7, 496−505

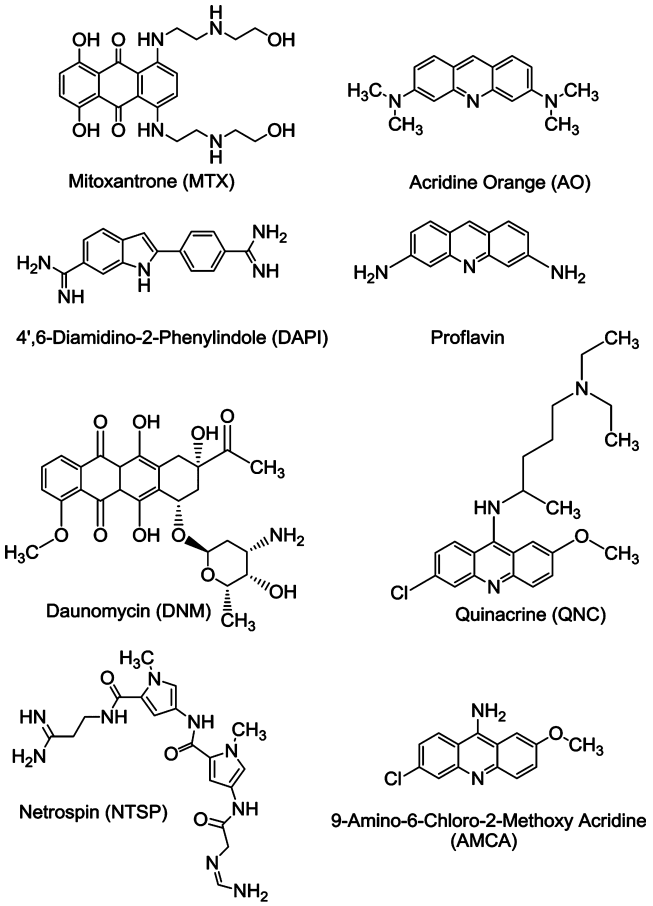

Figure 1. Structures of the small molecules known to have affinity for nucleic acids that were initially studied for binding to RNA 1×1 nucleotide internal loops *via* competition dialysis and various spectroscopic methods.

indole (DAPI) binds specifically to RNAs containing the 5′CAG/3′GAC motif (where the underlined A's indicate the internal loop) found in expanded r(CAG) repeats (r(CAG)^{exp}) that are associated with HD and SCA3. A virtual screen was completed in order to identify other compounds that are similar to DAPI in shape and chemistry alignment or the positioning of functional groups, rings, hydrophobic groups, charge, *etc.* The most potent small molecule, 4-guanidinophenyl 4-guanidinobenzoate, improves pre-mRNA splicing defects in patient-derived cells lines due to the sequestration of muscleblind-like 1 protein (MBNL1) by r(CAG)^{exp}.[17] Such studies provide useful leads for the development of chemical probes to study r(CAG)^{exp} toxicity as well as potential therapeutics that target r(CAG)^{exp}.

RESULTS AND DISCUSSION

Studying the Binding of Small Molecules to 1×1 Nucleotide RNA Internal Loops. Previous studies have shown that cell-permeable DNA-binding agents interact with RNAs containing 1×1 nucleotide internal loops.[15,16] Interestingly, 1×1 nucleotide internal loops are found multiple times in transcripts with expanded triplet repeats[18] and are associated with disorders such as DM1, HD, SCA3, and FXTAS. We therefore used competition dialysis[19] to evaluate the binding selectivity of various cell permeable DNA-binding agents for RNA 1×1 nucleotide internal loops and other nucleic acids. The small molecules used in competition dialysis studies include mitoxantrone (MTX), acridine orange (AO), DAPI, proflavin, daunomycin (DNM), quinacrine (QCN), 9-amino-6-chloro-2-methoxy acridine (ACMA), and netropsin (NTSP) (Figure 1). AO, proflavin, DNM, MTX, QCN, and ACMA bind DNA by intercalation.[20−23] MTX binds a hairpin structure in a *tau* (*MAPT*) pre-mRNA,[24] which has been implicated in Alzheimer's and other neurodegenerative diseases. A structure of MTX bound to *tau* hairpin has been reported.[25] Derivatives of AO and proflavin have been used as components of small molecules that bind RNAs as these structures intercalate into stretches of GC pairs.[26] DNM is related in structure to doxorubicin, which has been shown to bind to the HIV slippery sequence and inhibit frameshifting.[27] DAPI and netropsin either bind in the minor groove or have a mixed binding mode that includes minor groove binding and intercalation.[28−30] DAPI has been shown to bind group I introns and inhibit self-splicing.[31,32]

The nucleic acids used in these studies include each possible 1×1 nucleotide internal loop closed by two GC pairs (Figure 2).[33−35] The internal loops were embedded in a cassette containing a GNRA-type hairpin that ensures proper folding.[10,36] The 5′CUG/3′GUC, 5′CAG/3′GAC, and 5′CGG/3′GGC loops are present in the RNAs that cause DM1, HD and SCA3, and FXTAS, respectively.[37] A fully paired RNA was used as a control for ligands that bind to canonically paired RNAs helices.[38]

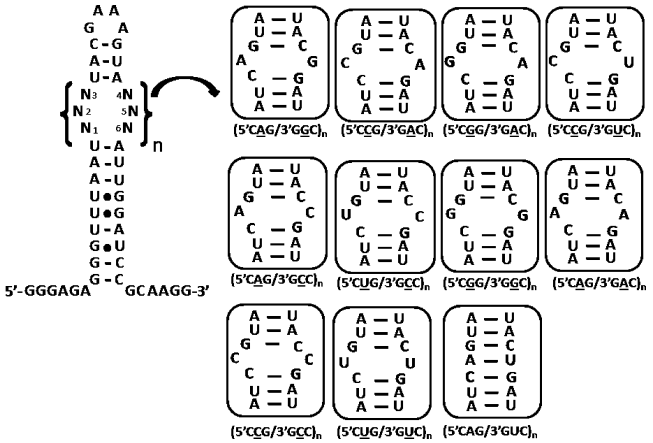

Figure 2. Secondary structures of the RNAs used to study the binding and selectivity of DNA-binding agents and related compounds. The nomenclature used for each of these RNAs is indicated below the secondary structure.

The results of competition dialysis studies are shown in Figure 3. Two ligands, proflavin and AO, show little preference for binding to a fully paired RNA or any of the RNAs with 1×1 nucleotide internal loops. This is perhaps not surprising since these ligands would most likely interact with RNA by intercalating between the consecutive GC pairs[22,39] common to all RNAs studied (Figure 2).

MTX, NTSP, and ACMA show modest binding preferences. MTX has a slight preference for 5′CCG/3′GAC while it discriminates against 5′CUG/3′GCC. In a previously reported NMR spectroscopy study of MTX bound to a *tau* pre-mRNA hairpin, MTX binds at the base of the stem between two GC pairs that flank a bulged A.[25] There is electrostatic complementarity between the MTX side chains and the major groove, which could also occur in the RNA with the

dx.doi.org/10.1021/cb200413a | *ACS Chem. Biol.* 2012, 7, 496−505

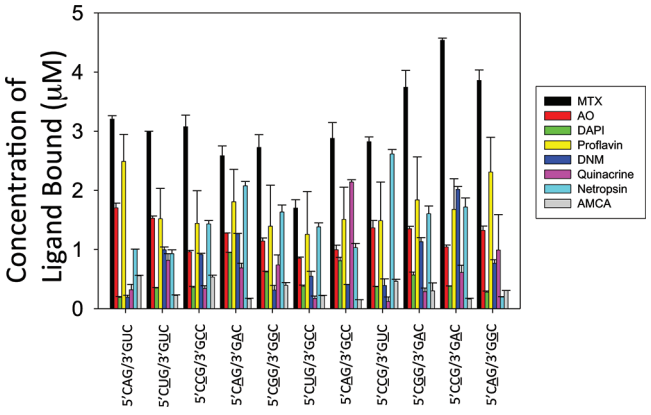

Figure 3. Data from competition dialysis used to study the binding of the ligands shown in Figure 1 to RNA structures shown in Figure 2. Competition dialysis experiments were completed by incubating one ligand with the RNAs indicated.

5′CCG/3′GAC motif. NTSP has a slight preference for 5′CCG/3′GUC over 5′CAG/3′GAC, 5′CGG/3′GAC, 5′CGG/3′GCC, and 5′CCG/3′GAC (which are greater than the remaining loops studied). It discriminates against 5′CAG/3′GGC. ACMA binds preferentially to the fully paired RNA and the RNA displaying 5′CCG/3′GCC slightly over 5′CCG/3′GUC

Clear binding preferences are observed for DNM, QNC, and DAPI. DNM prefers to bind 5′CCG/3′GAC with a stoichiometry of ~2:1 (based on the amount of bound ligand relative to the amount of RNA target), whereas QNC prefers to bind 5′CAG/3′GCC with an ~2:1 stoichiometry. DAPI preferentially binds to 5′CAG/3′GAC and 5′CAG/3′GCC in stoichiometric amounts. DAPI has been previously shown to bind the minor groove of AT steps in DNA and to intercalate at AU steps in RNA.[28] There is also evidence from NMR spectroscopy studies that DAPI intercalates between CG steps in DNA[28] and binds to the minor groove in DNAs containing T/T mismatches.[29]

Most interestingly, DAPI displayed selectivity for the 5′CAG/3′GAC motif. This motif periodically repeats in transcripts with r(CAG)^{exp} that are associated with HD, SCA3, and Kennedy's disease.[18] Like expanded r(CUG) repeats (r(CUG)^{exp}), r(CAG)^{exp} have recently been shown to bind and sequester MBNL1 leading to pre-mRNA splicing defects.[17] Therefore, the affinity of DAPI for RNAs containing various 1×1 nucleotide internal loops and a fully paired RNA was determined using fluorescence anisotropy (Table 1). In good agreement with the results of competition dialysis, DAPI binds most tightly to the RNA containing the 5′CAG/3′GAC motif (0.22 ± 0.06 μM). It binds approximately 2.5-fold more weakly to RNAs containing 5′CUG/3′GUC (0.55 ± 0.2 μM) and 5′CGG/3′GGC (0.50 ± 0.1 μM) and ~5-fold more weakly to an RNA with the 5′CCG/3′GCC motif (0.99 ± 0.2 μM). The K_D for binding to a fully paired RNA is >2 μM.

Identifying DAPI-like Small Molecules That Specifically Bind 1×1 Nucleotide A/A Internal Loops Using Virtual Screening. DAPI shows modest selectivity and reasonable binding affinity for an RNA containing a single copy of the 5′CAG/3′GAC motif that is associated with HD and SCA3. Therefore, we aimed to identify chemically similar compounds with improved affinities and selectivities. Virtual screening was used to identify ligands that have similar shape and chemistry alignment as DAPI. Chemistry alignment[40] accounts for the positioning of hydrogen bond donors, hydrogen bond acceptors, anions, cations, hydrophobic groups, and rings.

A 3D computational shape comparison between DAPI and a 250,000-member compound library available from the National Cancer Institute (NCI) was completed using the rapid overlay of chemical structures (ROCS) shape algorithm.[41] ROCS treats atoms as Gaussian functions and thus the overlap between two (or more) atoms are all Gaussian functions. This algorithm implemented in ROCS speeds up the 3-dimensional shape-based calculations, as it calculates the maximal intersection of the volumes of two molecules. The degree of shape similarity is quantified by the shape Tanimato coefficient[42] that ranges in values from 0 (no similarity) to 1 (complete shape similarity). Chemistry alignment is specified by the color force field (Implicit Mills Dean[40]) and is reported as the color score that has a range of 0 (no overlap) to 1 (complete chemistry alignment overlap). The combo score is the sum of the shape Tanimato coefficient and the color score. Nine compounds were selected for further investigation on the basis of their chemical diversity as determined by visual inspection (Table 3).

Determining the Selectivities of DAPI-like Compounds. Two of the nine compounds identified from the virtual screen have a single absorption band near 260 nm, making them incompatible with competition dialysis experiments. Therefore, the binding and selectivity of the remaining compounds were further investigated (Figure 4). Compounds D1, D2, and D3 show little binding preference as they bind a fully paired RNA and the RNAs with different 1×1 nucleotide internal loops similarly. D4 has the following binding preferences: 5′CCG/3′GAC > 5′CAG/3′GAC ≫ other RNAs; it binds approximately stoichiometrically to 5′CCG/3′GAC and 5′CAG/3′GAC. D7 is the most selective for 5′CAG/3′GAC and binds stoichiometrically. D9 shows little preference for most RNAs and discriminates against 5′CAG/3′GAC.

Optical Melting Experiments. The binding of DAPI and the compounds identified from the virtual screen to an RNA with the 5′CAG/3′GAC motif was also studied by optical melting (Table 2). In all cases, simple monophasic melting curves were obtained. The presence of DAPI and D2 increases the melting temperature to the greatest extent compared to the other compounds when 1 equiv of ligand is added (6 and 5 °C, respectively). The T_m increases more modestly for compounds D1, D4, D6, and D7 (2–3 °C). Greater increases in the T_m are

Table 1. Binding Constants (μM) for DAPI and DAPI-like Ligands for Nucleic Acid Targets

ligand	5′CAG/3′GUC	5′CAG/3′GAC	5′CUG/3′GUC	5′CGG/3′GGC	5′CCG/3′GCC
DAPI[a]	>2	0.22 ± 0.06	0.55 ± 0.2	0.50 ± 0.1	0.99 ± 0.2
D2[a]	>2	0.70 ± 0.08			
D6[b]		0.06 ± 0.03			

[a]These K_d's were measured by using a direct binding assay since the compounds are fluorescent. [b]This K_d was measured by using a competitive binding assay in which D2 was used as the fluorescent indicator.

dx.doi.org/10.1021/cb200413a | ACS Chem. Biol. 2012, 7, 496–505

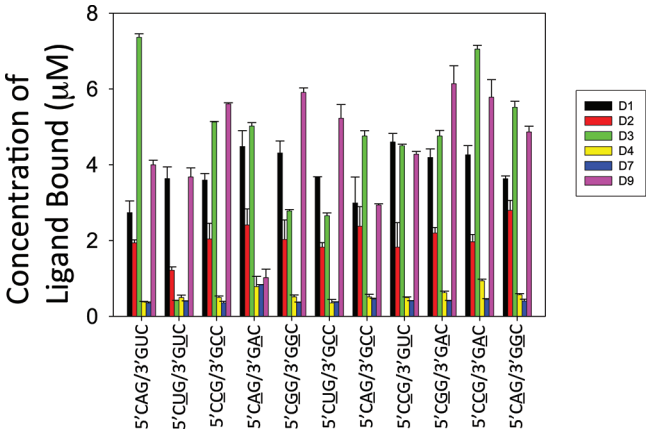

Figure 4. Data from competition dialysis used to study the compounds identified from virtual screening/chemical similarity searching. Only a subset of these compounds could be tested for binding using this method due to a lack of an absorbance band that is distinct from that of RNA.

Table 2. Change in Melting Temperature, ΔT_m, of an RNA Displaying the 5′CAG/3′GAC Motif in the Presence of Various Ligands

compound	ΔT_m (1 equiv)	ΔT_m (2 equiv)
DAPI	6	10
D1	2	4
D2	5	10
D4	2	5
D6	3	9
D7	3	8

observed when 2 equiv of the ligand are added: 4−5 °C for D1 and D4, 8−10 °C for DAPI, D2, D6, and D7. The increases in T_m indicate that the small molecules bind to the RNA and increase its thermodynamic stability.

Inhibition of the r(CAG)^{exp}−MBNL1 Complex by Small Molecules. A recent report showed that r(CAG)^{exp} mimics r(CUG)^{exp} in the misregulation of alternative splicing.[17] r(CUG)^{exp} cause myotonic dystrophy type 1 (DM1) *via* an RNA gain-of-function mechanism.[37] Specifically, the toxic r(CUG)^{exp} present in the 3′ untranslated region of the dystrophia myotonica protein kinase (*DMPK*) mRNA[37,43,44] binds to and inactivates MBNL1. Sequestration of MBNL1 by r(CUG)^{exp} causes mis-splicing of various pre-mRNAs in muscles including cardiac troponin T (cTNT), the insulin receptor (INSR), and the muscle-specific chloride ion channel (CLCN1).[45] Each of these splicing defects explains physiological phenotypes of DM1 such as insulin insensitivity and myotonia.

Several other studies have shown that r(CAG)^{exp} cause toxicity by the same gain-of-fucntion mechanism.[46−49] In particular, (i) r(CAG)^{exp} interacts with MBNL1 and forms nuclear foci in cells and animal models;[17,50−52] (ii) recombinant MBNL1 binds r(CAG)^{exp} and r(CUG)^{exp} with similar affinities;[14,17] and (iii) r(CAG)^{exp} has been found to be toxic in *Drosophila* models when an untranslated r(CAG)^{exp} is expressed.[53]

Therefore, we determined if DAPI and the DAPI-like compounds could disrupt the r(CAG)^{exp}−MBNL1 complex using a time-resolved FRET (TR-FRET) assay. Briefly, 5′-biotinylated r(CAG)$_{12}$ and MBNL1-His$_6$ are pre-equilibrated and incubated with the compound of interest. Next, streptavidin-XL665 (binds to the biotinylated RNA oligonucleotide) and Tb-Anti-His$_6$ (binds to MBNL1) are added. If the compound does not disrupt the r(CAG)$_{12}$−MBNL1 interaction, then XL665 and Tb are within close enough proximity to form a FRET pair and TR-FRET can be measured. Conversely, TR-FRET is not observed if the compound inhibits formation of the r(CAG)$_{12}$−MBNL1 complex. It should be noted that the RNA−protein complex is pre-formed prior to addition of the compound of interest. Therefore, in order to be scored as an active compound, the small molecule must displace MBNL1 from r(CAG) repeats.

The IC$_{50}$'s measured for the DAPI-like compounds range from >1000 to 3 μM (Table 3). The least potent compounds have the least amount of charge and hydrophobic surface area with which to interact with RNA while the most potent compounds contain the most charge and the largest hydrophobic surface area. The most potent compound, D6, is at least 20-fold more potent than the other compounds studied and contains two benzylguanidine side chains linked by an ester (Table 3). D6 binds to an RNA with a single copy of the 5′CAG/3′GAC motif with a dissociation constant of 60 nM as determined by fluorescence anisotropy (Table 1).

Compounds That Bind 5′CAG/3′GAC and Inhibit the r(CAG)-MBNL1 Complex Improve pre-mRNA Splicing Defects in Cell-Based Assays. A recent report showed that r(CAG)^{exp} mimics the misregulation of pre-mRNA alternative splicing that is observed for r(CUG)^{exp} in different cellular model systems.[17] We determined that the pre-mRNAs of the *NCOR2* and *ATP2A1* genes are mis-spliced in both DM1- and HD-derived fibroblast cells expressing different lengths of r(CUG)^{exp} and r(CAG)^{exp}, respectively (Supplemental Figure S-11A and S-12). Moreover, the alternative splicing each of these pre-mRNAs is MBNL1-sensitive in HEK293, as was determined by overexpression of MBNL1 (Supplemental Figure S-11C and D). Therefore these splicing markers were used to study the bioactivity of DAPI and DAPI-like compounds in HD patient-derived (r(CAG)69) and control fibroblasts. We also used an artificial model system of HD in which a neuroblastoma cell line stably expresses r(CAG)^{exp} (rCAG(74)).[17] In this cell line, the splicing of *NCOR2*, *ATP2A1*, and *MAPT* pre-mRNAs is abnormally shifted toward a DM-like pattern (Figure 5C and D and Supplemental Figure S-12).

As an initial screen, several DAPI-like compounds were incubated at the same concentration with both cellular models (100 μM), and their effects on cell morphology (an estimate of toxicity) and on *ATP2A1* splicing (an estimate of bioactivity) were determined (Supplemental Figures S-9 and S-10). D6 showed the least amount of toxicity as assessed by cell morphology (Figure 5A) and most significantly improved *ATP2A1* mis-splicing (Figure 5B). In contrast, DAPI showed the strongest morphological changes (Supplemental Figure S-9) and exacerbated splicing abnormalities of *ATP2A1* (Supplemental Figures S-9 and S-10). Interestingly, the structure of D6 is somewhat similar to pentamidine, which has been shown to improve DM1-associated pre-mRNA splicing defects in cellular and animal models of myotonic dystrophy.[54]

Next, we determined if D6 could improve other pre-mRNA splicing defects in HD fibroblasts (express r(CAG)69) and the neuroblastoma model system (expresses r(CAG)74). Dose responses were completed for improvement of the mis-splicing

dx.doi.org/10.1021/cb200413a | ACS Chem. Biol. 2012, 7, 496−505

Table 3. Structures of DAPI-like Compounds Identified from a Virtual Screen and the Corresponding Shape Tanimato Coefficients, Color Scores, Combo Scores, and IC_{50}'s

Compound ID	Structure	Shape Tanimato	Colored Score	Combo Score	IC_{50} (μM)
D1	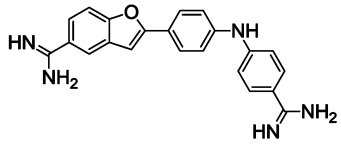	0.78	0.48	1.22	60
D2	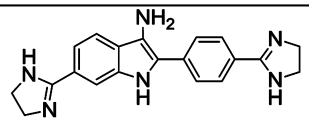	0.86	0.78	1.64	>125
D3	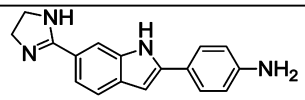	0.90	0.63	1.53	ND[a]
D4	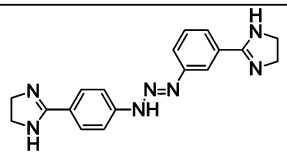	0.77	0.55	1.32	60
D5	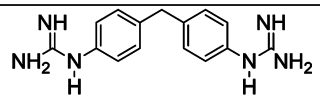	0.75	0.42	1.17	500
D6	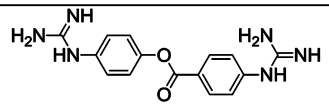	0.87	0.57	1.44	3
D7	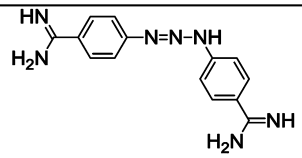	0.88	0.60	1.35	60
D8	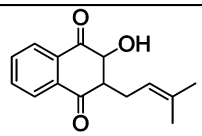	0.82	0.43	1.25	ND[a]
D9	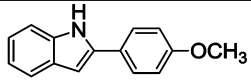	0.87	0.40	1.27	>1000

[a]The IC_{50} could not be measured because the compound interfered with the FRET measurements.

of *NCOR2* and *ATP2A1* in HD fibroblasts and of *NCOR2*, *ATP2A1*, and *MAPT* in the neuroblastoma cell line (Figure 5B, C, and D). Statistically significant improvement of *NCOR2* mis-splicing was observed when HD fibroblasts were treated with 50−300 μM D6. Likewise, improvement in *ATP2A1* mis-splicing was observed when cells were treated with 100−300 μM D6. In good agreement with the results observed in the HD fibroblasts, statistically significant improvement in the mis-

dx.doi.org/10.1021/cb200413a | *ACS Chem. Biol.* 2012, 7, 496−505

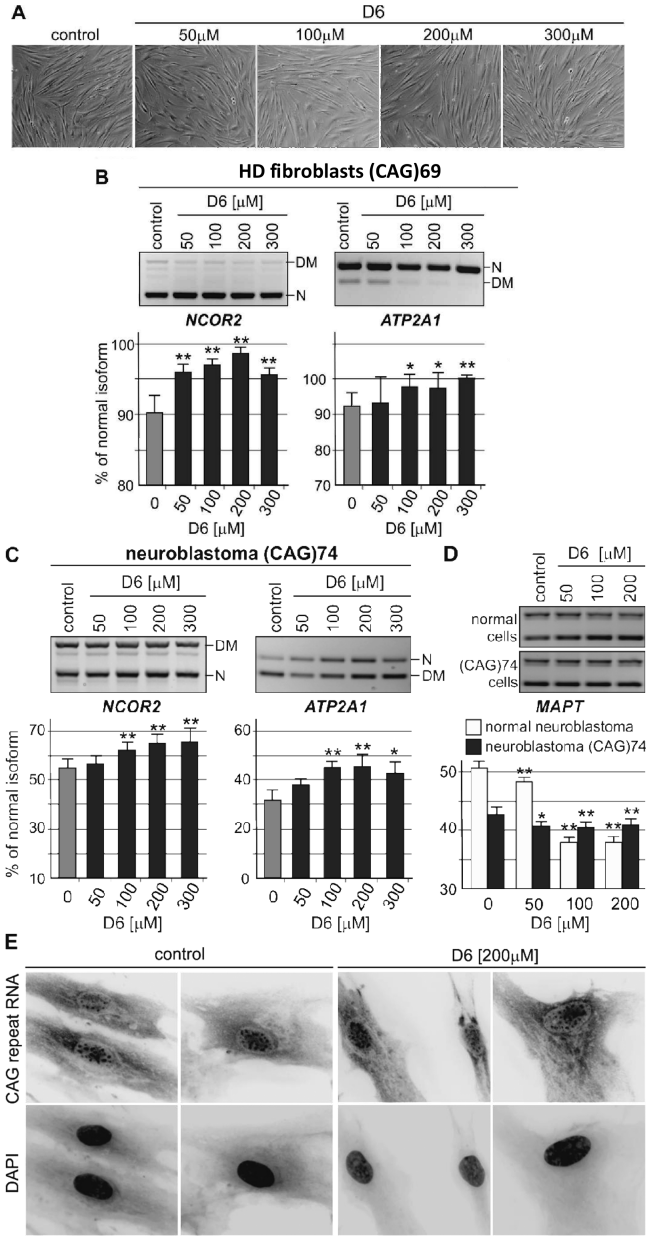

Figure 5. D6 corrects pre-mRNA splicing defects associated with sequestration of MBNL1 by r(CAG)^{exp}. (A) Microscopic images that show cell morphology is not affected by increasing concentrations of D6. (B) D6 improves pre-mRNA splicing defects in an HD patient-derived cell line. Statistically significant improvement of splicing is observed for both pre-mRNAs tested when the cells are treated with 100−300 μM D6. (C) D6 improves pre-mRNA splicing defects in neuroblastoma cells that stably express r(CAG)74. Statistically significant improvement of splicing is observed for both pre-mRNAs tested when the cells are treated with 100−300 μM D6. (D) D6 shifts the splicing of *MAPT* pre-mRNA toward the DM phenotype in both r(CAG)-expressing and normal neuroblastoma cells. (E) Fluorescence *in situ* hybridization (FISH) images using fluorescence microscopy show that D6 does not disrupt the formation of nuclear r(CAG)^{exp} foci in HD-derived fibroblasts (upper panels). Cell nuclei were stained with DAPI (lower panels); * indicates $P < 0.05$, and ** indicates $P < 0.01$. RT-PCR bands representing both normal (N) and DM-like (DM) splicing isoforms are indicated on the sides of gel images.

splicing of *NCOR2* and *ATP2A1* was also observed in the neuroblastoma cell line (Figure 5C). Gratifyingly, D6 was found to be the most potent inhibitor of the MBNL1-r(CAG)^{exp} complex, however, *in vitro* potency may not always correlate with bioactivity due to factors that may include compound toxicity and cellular uptake.

Unexpectedly, D6 slightly worsens the splicing of the *MAPT* pre-mRNA toward the DM-like phenotype in the neuroblastoma cell line express 74 r(CAG) repeats (Figure 5D). A more pronounced effect is observed when a normal neuroblastoma cell line is treated with D6 (Figure 5D). This may be due to D6 binding to the pre-mRNA and affecting the splicing outcome. Improved second-generation compounds can be developed to minimize these potential off target effects. Importantly, D6 does not affect the splicing of pre-mRNAs of other transcripts in control cell lines that do not express toxic r(CAG)^{exp} (Supplemental Figure S-12). Taken together, these results suggest that D6 inhibits the r(CAG)^{exp}-MBNL1 complex *in vivo* with at minimum modest specificity, increasing the concentration of free MBNL1 and improving splicing defects.

As is observed in DM1-affected cells,[55−58] the presence of r(CAG)^{exp} leads to formation of nuclear RNA foci (Figure 5E).[17] Therefore, we also determined if D6 could disrupt nuclear RNA foci formation in r(CAG)^{exp}-expressing cells. To measure this phenotype, fluorescence *in situ* hybridization (FISH) was employed using a fluorescently labeled hybridization probe that binds to r(CAG)^{exp}.[17] As shown in Figure 5E, D6 does not significantly affect the number or the intensity of nuclear r(CAG)^{exp} foci even though D6 improves splicing defects. Other studies, however, have described similar results in which nuclear foci and normal splicing patterns are observed in cell lines expressing r(CUG)^{exp}.[59,60] These results suggest that D6 displaces enough MBNL1 to improve splicing defects but not enough MBNL1 or other proteins [50,55,57,58] to disrupt nuclear RNA foci.

Summary and Outlook. A bioactive small molecule was identified that improves splicing defects associated with expanded r(CAG) repeats. The compound was identified by investigating the RNA-binding preferences for a series of small molecules with known affinity for nucleic acids. A lead molecule that binds 5′CAG/3′GAC, DAPI, was optimized by virtually screening a database of small molecules for compounds that are similar in shape and chemistry alignment. Specifically, compound D6 (Table 3) inhibits the r(CAG)−MBNL1 complex formation *in vitro* and improves a subset of pre-mRNA splicing defects that are associated with formation of the r(CAG)^{exp}−MBNL1 complex *in vivo*. This approach could yield small molecules that specifically target other RNAs in general and other repeating transcripts in particular. The potency and specificity of the compounds could be improved using a modular assembly strategy.[13,14,16,61]

Although many studies have shown that r(CAG)^{exp} causes splicing defects and toxicity due to an RNA gain-of-function,[17,50,53] other studies have disregarded the pathogenic role of r(CAG)^{exp} transcripts on nuclear foci formation[62] or mis-splicing.[50] Thus, the identification of a small molecule that targets r(CAG)^{exp}, freeing MBNL1, and improving splicing defects, would provide further evidence of a dominant RNA gain-of-function mechanism. This compound could also provide a chemical probe to better understand the mechanisms associated with r(CAG)^{exp} toxicity.

METHODS

RNA Preparation and Purification. The RNA used in TR-FRET assays (5′biotinylated-$(CAG)_{12}$) was purchased from Dharmacon. The

dx.doi.org/10.1021/cb200413a | *ACS Chem. Biol.* 2012, 7, 496−505

ACE protecting groups were cleaved using Dharmacon's deprotection buffer. The sample was lyophilized, dissolved in Milli-Q water, and desalted using a PD-10 gel filtration column (GE Healthcare). RNAs used in competition dialysis and fluorescence anisotropy experiments were prepared *via* run off-transcription using synthetic DNA templates (Integrated DNA Technologies, Inc.) and a Stratagene RNAMaxx transcription kit. They were purified by denaturing polyacrylamide gel electrophoresis as previously described[34] and dissolved in 1X Competition Dialysis Buffer (8 mM NaH_2PO_4, 185 mM NaCl and 1 mM EDTA; pH 7.2).

Oligonucleotide concentrations were determined by absorbance at 260 nm (90 °C for the RNA used in TR-FRET assays; RT for RNAs used in competition dialysis) using a Beckman Coutler DU800 UV−vis spectrophotometer equipped with a Peltier temperature controller unit. Oligonucleotide extinction coefficients were determined using HyTher version 1.0 (Nicolas Peyret and John SantaLucia, Jr., Wayne State University, Detroit, MI).[63,64] The parameters used by HyTher were calculated using information on the extinction coefficients of nearest neighbors in RNA.[65]

Ligands. All ligands, *viz.*, mitoxantrone (MTX), acridine orange (AO), proflavin,4′,6-diamidino-2-phenylindole (DAPI), netrospin (NTSP), daunomycin (DNM), quinacrine (QNC) and 9-amino 6-chloro 2-methoxy acridine (ACMA), were dissolved in Milli-Q water. The concentrations of the ligands were determined by UV absorbance spectroscopy using their respective extinction coefficients at their absorbance maxima (608, 430, 296, 353, 444, 480, 424, and 430 nm for MTX, AO, NTSP, DAPI, proflavin, DNM, QNC, and ACMA, respectively). DAPI-like compounds were procured from NCI (Table 3) and were purified by high performance liquid chromatography before use. HPLC traces and mass spectra for all compounds are provided in the Supporting Information.

Competition Dialysis. Pierce Slide-A-Lyzer MINI dialyzer units (Pierce Biotechnology, Inc.) were dialyzed against water for 24 h in order to ensure that the units did not leak. Competition dialysis was completed as previously described by Chaires.[22] Briefly, RNAs were folded by heating at 60 °C for 5 min followed by slowly cooling to room temperature on the benchtop. Dialysis units containing 0.1 mL of 1.6 μM RNA were placed in 200 mL of 1 μM ligand in 1X Competition Dialysis Buffer. The samples were allowed to equilibrate with the dialysate by stirring at 200 rpm for 24 h at room temperature (20−22 °C). Previous studies have shown that this is sufficient time for the sample to reach equilibrium.[19]

At the end of the equilibration period, 67.5 μL of each sample was carefully removed from the dialyzer unit and transferred to a microcentrifuge tube. To each sample, 7.5 μL of 10% (w/v) sodium dodecyl sulfate (SDS) was added to give a final concentration of 1% (w/v) SDS, which is sufficient to dissociate the ligand. The SDS step was completed to ensure accurate determination of the concentration of bound ligand as the spectroscopic properties of the bound ligand could be different from that of unbound. The total ligand concentration (C_t) within each dialysis unit was determined spectrophotometrically using the appropriate absorbance wavelength and extinction coefficient for each compound. Appropriate corrections were made for the small dilution resulting from the addition of SDS.

The free ligand concentration (C_f) was determined from an aliquot of the dialysate solution, which did not vary appreciable from the initial 1 μM. The bound ligand concentration (C_b) was then determined using eq 1:

$$C_b = C_t - C_f \tag{1}$$

where C_b, C_t, and C_f are concentrations of bound, total, and free ligand, respectively.

Affinity Measurements Using Fluorescence Anisotropy. Fluorescence anisotropy measurements were performed on a Molecular Devices SpectraMax M5 microplate reader using an excitation wavelength of 368 nm and emission wavelength of 500 nm. Measurements were performed in a buffer solution containing 20 mM HEPES, pH 7.5, 5 mM KCl, 150 mM NaCl, and 1 mM $MgCl_2$ (1X Affinity Buffer). The RNA of interest was folded by heating at 60 °C for 5 min in 1X Affinity Buffer followed by slowly cooling to room temperature on the benchtop.

For direct measurements, the RNA was titrated into 50 nM compound of interest in 1X Affinity Buffer with a 5 min equilibration time between additions. Anisotropy was measured as a function of RNA concentration and fit to eq 2:

$$A = A_0 + 0.5\Delta\epsilon\{(([L_0] + [RNA]_0) + K_t) - (([L]_0 + [RNA]_0) + K_t))^2 - 4[L]_0 [RNA]_0)^{0.5}\} \tag{2}$$

where A is the observed anisotropy, A_0 is the fluorescence anisotropy in the absence of RNA, $\Delta\varepsilon$ is the difference between the fluorescence intensity in the absence of RNA and the fluorescence anisotropy in the presence of infinite RNA concentration, $[L]_0$ is the concentration of ligand, $[RNA]_0$ is the concentration of the RNA of interest, and K_t is the dissociation constant.

For competition measurements, the RNA of interest was added to 50 nM D2 until saturation was reached. Then, the compound of interest was titrated into the solution, and the anisotropy was measured after a 5 min equilibration period. The fraction of ligand bound as a function of compound was fit to eq 3:

$$\theta = \frac{1}{2[L]_0}\left[K_t + \frac{K_t}{K_d}[C_t]\right] + [RNA] + [L] - \sqrt{K_t + \frac{K_t}{K_d} + [C_t] + [RNA] + [L]^2 - 4[L][RNA]} \tag{3}$$

where θ is the fraction of D2 bound, K_t is the dissociation constant for D2 as determined from direct measurements, K_d is the dissociation constant for the competing DAPI-like compound, $[C_t]$ is the concentration of competing DAPI-like compound, $[L]$ is the concentration of D2, $[RNA]$ is the concentration of RNA required to reach saturation.

Optical Melting Experiments. Optical melting curves were obtained using a Beckman Coulter DU 800 spectrometer. The temperature of the cell holder was regulated by using a peltier heater. The RNAs were first denatured in 1X Affinity Buffer by heating to 90 °C and cooling to 15 °C. The absorbance at 260 nm as a function of temperature was recorded using a rate of 1 °C/min. The melting temperature, T_m, was calculated using eq 4:

$$T_m = \frac{\Delta H^\circ \times 1000}{\Delta S^\circ} - 273.15 \tag{4}$$

where ΔH° and ΔS° are the changes in enthalpy and entropy, respectively.

Quantitative Time-Resolved Fluorescence Resonance Energy Transfer (TR-FRET) Assay. The TR-FRET assay used to identify lead inhibitors of the $r(CAG)_{12}$−MBNL1 complex is based on PubChem BioAssay AID 2675. Briefly, 5′-biotinylated $r(CAG)_{12}$ was folded in 1X Folding Buffer (20 mM HEPES, pH 7.5, 110 mM KCl, and 10 mM NaCl) by heating at 60 °C followed by slowly cooling to room temperature on the benchtop. The buffer was adjusted to 1X Assay Buffer (20 mM HEPES, pH 7.5, 110 mM KCl, 10 mM NaCl, 2 mM $MgCl_2$, 2 mM $CaCl_2$, 5 mM DTT, 0.1% BSA, and 0.5% Tween-20) and MBNL1-His_6 was added. The final concentrations of RNA and MBNL1 were 80 nM and 60 nM, respectively. The sample was allowed to equilibrate at room temperature for 5 min, and then the compound of interest was added. After 15 min, streptavidin-XL665 and anti-His_6-Tb antibody were added to final concentrations of 40 nM and 0.44 ng/μL, respectively, in a total of 10 μL. The samples were incubated for 1 h at room temperature and then transferred to a well of a black 96-well plate. Time-resolved fluorescence was measured on a Molecular Devices SpectraMax M5 plate reader. Fluorescence was first measured using an excitation wavelength of 345 nm and an emission wavelength of 545 nm (fluorescence due to Tb). TR-FRET was then measured by using an excitation wavelength of 345 nm, an emission wavelength of 665 nm, a 200 μs evolution time, and a 1.5 ms

dx.doi.org/10.1021/cb200413a | *ACS Chem. Biol.* 2012, 7, 496−505

integration time. The ratio of fluorescence intensity of 545 and 665 nm as compared to the ratios in the absence of ligand and in the absence of RNA were used to determine IC_{50}'s.

Virtual Screening of the NCI Database for DAPI-like Compounds. Virtual screening was performed using a Mac OSX 10.6 operating system with a 2.8 GHz Quad-Core Intel Xeon W3530 "Nehalem" processor and 6 GB of memory. As a starting point for the virtual screen, Chem3D (Cambridge software) was used to energy-minimize (MMFF94force field) a 3-dimensional conformer of DAPI. Omega 2.3.2 (v 2.02) was then used to generate 100 conformers of the query molecule using an energy window of 10 kcal and an rmsd of 0.8 Å. Up to 100 conformers of each molecule in the NCI database were also generated. 3D-shape comparisons (shape Tanimoto coefficient) were completed using rapid overlay of chemical structure (ROCS, version 3.0.0) while the chemistry alignment overlap (color score) was completed by using the color force field (Implicit Mills Dean[40]) from the OpenEye software package. The combo score is the sum of the shape Tanimoto coefficient and the color score.

Cell Culture. Fibroblasts derived from an unaffected individual (GM07492 line), HD patient (GM04281 line expressing *HTT* gene with normal repeat tract, r(CAG)17, and expanded repeats, r(CAG)-69) as well as myotonic dystrophy type 1 probands (GM03987, GM04033 and GM03989 lines expressing mutant *DMPK* transcript containing ~500, ~1000, and ~2000 CUG repeat tracts, respectively) were obtained from the Coriell Cell Repositories. Human Neuronal Epithelioma cell line, SK-N-MC (neuroblastoma) and SK-N-MC with stable expression of 74 CAG repeats in 3'UTR of EGFP reporter gene (neuroblastoma (CAG)74)[17] were a gift from Professor Wlodzimierz J. Krzyzosiak (Institute of Bioorganic Chemistry, Polish Academy of Sciences in Poznan, Poland). All fibroblast cell lines were maintained in MEM medium (Invitrogen) supplemented with 10% FBS (Sigma), 1X antibiotic antimycotic solution (Sigma) and 1X MEM nonessential amino acid solution (Sigma). Neuroblastoma and HEK293 cells were grown in 1X DMEM medium (Invitrogen) supplemented with 10% FBS and 1X antibiotic antimycotic solution. Overexpression of MBNL1 protein was performed in HEK293 cells grown on 4 cm plates (~60% confluence) transfected with 1.5 μg of plasmid coding EGFP-MBNL1 fusion protein using Lipofectamine 2000 reagent (Invitrogen) according to the manufacturer's instructions. After 48 h, cells were harvested, and RNA was isolated.

Treatment of Cell Lines with Small Molecules. Fibroblast and SK-N-MC cells were seeded in 6-well plates in complete medium (as above) and grown to ~60% confluence. Then, fresh medium containing the small molecule of interest was added at different final concentrations (50−300 μM). For untreated cells, the same volume of water was added. After 48 h, cells were harvested, and total RNA was isolated.

RT-PCR Splicing Assays. Total RNA was isolated from cells using TRI Reagent (Sigma) according to the manufacturer's instructions. RNA concentration was measured by NanoDrop spectrophotometer. Approximately 1 μg of total RNA was reverse transcribed using a Superscript III kit (Invitrogen) and random primers (Promega) according to manufacturer's recommendations. All cDNAs were diluted 5-fold with water prior to PCR. GoTaq Flexi DNA Polymerase (Promega) and 0.1 mM dNTP mix, 1.5 mM $MgCl_2$, 1 μM of each primer were used for RT-PCR assays. Please see the Supporting Information for the primers and cycling conditions used to determine the splicing products for each transcript (Supplemental Table S-1).

The products of PCR amplification were separated using a 2% agarose gel in 1X TBE buffer. The gels were stained with 0.5 μg/mL ethidium bromide and imaged. Each cDNA sample was assayed in three or six independent RT-PCR reactions. The fractions of alternative splicing isoforms were calculated by dividing the intensity of PCR product band corresponding to the normal splicing variant (opposite of the DM isoform) by the total intensity of both splicing forms. Statistical significance was assessed using the average percentage (±SD) of the normal isoform obtained from at least six independent experiments in comparison the average percentage (±SD) of untreated cells. Statistical significance was determined by a two-tailed *t* test using Microsoft Excel (* for $P < 0.05$ and ** for $P < 0.01$).

Fluorescence *in Situ* Hybridization (FISH). For RNA fluorescence *in situ* hybridization (FISH) experiments, treated and untreated fibroblasts were grown on coverslips and then fixed in 4% PFA/PBS at 4 °C and washed three times with 1X PBS. The cells were prehybridized with 30% formamide and 2X SSC for 10 min, followed by hybridization in buffer containing 30% formamide, 2X SSC, 0.02% BSA, 66 mg/mL yeast tRNA (Ambion), 480 U/mL RNasin (Promega) and 2 ng/mL DNA/LNA probes (CTG)6-CA. The probe was labeled at the 5'-end with Cy3 and modified at positions 2, 5, 8, 13, 16, and 19 with LNA residues. Posthybridization washing was completed in 30% formamide and 2X SSC at 45 °C for 30 min followed by 1x SSC at 37 °C for the next 30 min. FISH images were acquired on a Zeiss Axioskop 2 Plus microscope (zoom 630x) equipped with a AxioCam HRm camera and processed with AxioVision Release 4.6 software.

■ ASSOCIATED CONTENT

Supporting Information

This material is free *via* the Internet at http://pubs.acs.org.

■ AUTHOR INFORMATION

Corresponding Author

*E-mail: ksobczak@wp.pl; disney@scripps.edu.

■ ACKNOWLEDGMENTS

This work was funded by the National Institutes of Health (3R01GM079235-02S1 and 1R01GM079235-01A2 to M.D.D.) and the Polish Ministry of Science and Higher Education grant N302 260938. M.D.D. is a Camille & Henry Dreyfus New Faculty Awardee, a Camille & Henry Dreyfus Teacher-Scholar, and a Research Corporation Cottrell Scholar.

■ ABBREVIATIONS

AMCA, 9-amino-6-chloro-2-methoxy acridine; AO, acridine orange; ATP2A1, sarcoplasmic/endoplasmic reticulum calcium ATPase 1; DAPI, 4′,6-diamidino-2-phenylindole; DM1, myotonic dystrophy type 1; *DMPK*, dystrophia myotonica protein kinase; DNM, daunomycin; FISH, fluorescence *in situ* hybridization; FXTAS, Fragile X-associated Tremor Ataxia Syndrome; HD, Huntington's disease; IC_{50}, half-maximal inhibitory concentration; K_d, disociation constant; *MAPT*, microtubule-associated protein tau; MBNL1, muscleblind-like 1 protein; MTX, mitoxantrone; NCI, National Cancer Institute; *NCOR2*, nuclear receptor corepressor 2; NTSP, netropsin; QCN, quinacrine; $r(CAG)^{exp}$, expanded r(CAG) repeats; $r(CUG)^{exp}$, expanded r(CUG) repeats; ROCS, rapid overlay of chemical structures; SCA3, spinocerebellar ataxia type 3

■ REFERENCES

(1) Doudna, J. A. (2000) Structural genomics of RNA. *Nat. Struct. Biol. 7* (Suppl.), 954−956.

(2) Batey, R. T., Rambo, R. P., and Doudna, J. A. (1999) Tertiary motifs in RNA structure and folding. *Angew. Chem., Int. Ed. 38*, 2326−2343.

(3) Zaug, A. J., and Cech, T. R. (1986) The intervening sequence RNA of Tetrahymena is an enzyme. *Science 231*, 470−475.

(4) Lagos-Quintana, M., Rauhut, R., Lendeckel, W., and Tuschl, T. (2001) Identification of novel genes coding for small expressed RNAs. *Science 294*, 853−858.

(5) Winkler, W., Nahvi, A., and Breaker, R. R. (2002) Thiamine derivatives bind messenger RNAs directly to regulate bacterial gene expression. *Nature 419*, 952−956.

(6) Nissen, P., Hansen, J., Ban, N., Moore, P. B., and Steitz, T. A. (2000) The structural basis of ribosome activity in peptide bond synthesis. *Science 289*, 920−930.
(7) Gallego, J., and Varani, G. (2001) Targeting RNA with small-molecule drugs: therapeutic promise and chemical challenges. *Acc. Chem. Res. 34*, 836−843.
(8) Hamy, F., Felder, E. R., Heizmann, G., Lazdins, J., Aboul-ela, F., Varani, G., Karn, J., and Klimkait, T. (1997) An inhibitor of the Tat/TAR RNA interaction that effectively suppresses HIV-1 replication. *Proc. Natl. Acad. Sci. U.S.A. 94*, 3548−3553.
(9) Mathews, D. H., Disney, M. D., Childs, J. L., Schroeder, S. J., Zuker, M., and Turner, D. H. (2004) Incorporating chemical modification constraints into a dynamic programming algorithm for prediction of RNA secondary structure. *Proc. Natl. Acad. Sci. U.S.A. 101*, 7287−7292.
(10) Mathews, D. H., Sabina, J., Zuker, M., and Turner, D. H. (1999) Expanded sequence dependence of thermodynamic parameters improves prediction of RNA secondary structure. *J. Mol. Biol. 288*, 911−940.
(11) Woese, C. R., Magrum, L. J., Gupta, R., Siegel, R. B., Stahl, D. A., Kop, J., Crawford, N., Brosius, J., Gutell, R., Hogan, J. J., and Noller, H. F. (1980) Secondary structure model for bacterial 16S ribosomal RNA: phylogenetic, enzymatic and chemical evidence. *Nucleic Acids Res. 8*, 2275−2293.
(12) Disney, M. D., Lee, M. M., Pushechnikov, A., and Childs-Disney, J. L. (2010) The role of flexibility in the rational design of modularly assembled ligands targeting the RNAs that cause the myotonic dystrophies. *ChemBioChem 11*, 375−382.
(13) Lee, M. M., Childs-Disney, J. L., Pushechnikov, A., French, J. M., Sobczak, K., Thornton, C. A., and Disney, M. D. (2009) Controlling the specificity of modularly assembled small molecules for RNA via ligand module spacing: targeting the RNAs that cause myotonic muscular dystrophy. *J. Am. Chem. Soc. 131*, 17464−17472.
(14) Lee, M. M., Pushechnikov, A., and Disney, M. D. (2009) Rational and modular design of potent ligands targeting the RNA that causes myotonic dystrophy 2. *ACS Chem. Biol. 4*, 345−355.
(15) Cho, J., Hamasaki, K., and Rando, R. R. (1998) The binding site of a specific aminoglycoside binding RNA molecule. *Biochemistry 37*, 4985−4992.
(16) Pushechnikov, A., Lee, M. M., Childs-Disney, J. L., Sobczak, K., French, J. M., Thornton, C. A., and Disney, M. D. (2009) Rational design of ligands targeting triplet repeating transcripts that cause RNA dominant disease: application to myotonic muscular dystrophy type 1 and spinocerebellar ataxia type 3. *J. Am. Chem. Soc. 131*, 9767−9779.
(17) Mykowska, A., Sobczak, K., Wojciechowska, M., Kozlowski, P., and Krzyzosiak, W. J. (2011) CAG repeats mimic CUG repeats in the misregulation of alternative splicing. *Nucleic Acids Res. 39*, 8938−8951.
(18) Sobczak, K., Michlewski, G., de Mezer, M., Kierzek, E., Krol, J., Olejniczak, M., Kierzek, R., and Krzyzosiak, W. J. (2010) Structural diversity of triplet repeat RNAs. *J. Biol. Chem. 285*, 12755−12764.
(19) Chaires, J. B., Ragazzon, P. A., Garbett, N. C. (2003) A competition dialysis assay for the study of structure-selective binding to nucleic acids, in *Current Protocols in Nucleic Acid Chemistry*, Unit 8.3, John Wiley and Sons, Inc., New York.
(20) Li, N., Ma, Y., Yang, C., Guo, L., and Yang, X. (2005) Interaction of anticancer drug mitoxantrone with DNA analyzed by electrochemical and spectroscopic methods. *Biophys. Chem. 116*, 199−205.
(21) Lyles, M. B., and Cameron, I. L. (2002) Interactions of the DNA intercalator acridine orange, with itself, with caffeine, and with double stranded DNA. *Biophys. Chem. 96*, 53−76.
(22) Neidle, S., Pearl, L. H., Herzyk, P., and Berman, H. M. (1988) A molecular model for proflavine-DNA intercalation. *Nucleic Acids Res. 16*, 8999−9016.
(23) Wang, A. H., Ughetto, G., Quigley, G. J., and Rich, A. (1987) Interactions between an anthracycline antibiotic and DNA: molecular structure of daunomycin complexed to d(CpGpTpApCpG) at 1.2-Å resolution. *Biochemistry 26*, 1152−1163.
(24) Liu, Y., Peacey, E., Dickson, J., Donahue, C. P., Zheng, S., Varani, G., and Wolfe, M. S. (2009) Mitoxantrone analogues as ligands for a stem-loop structure of tau pre-mRNA. *J. Med. Chem. 52*, 6523−6526.
(25) Zheng, S., Chen, Y., Donahue, C. P., Wolfe, M. S., and Varani, G. (2009) Structural basis for stabilization of the tau pre-mRNA splicing regulatory element by novantrone (mitoxantrone). *Chem. Biol. 16*, 557−566.
(26) Carlson, C. B., Vuyisich, M., Gooch, B. D., and Beal, P. A. (2003) Preferred RNA binding sites for a threading intercalator revealed by *in vitro* evolution. *Chem. Biol. 10*, 663−672.
(27) Marcheschi, R. J., Mouzakis, K. D., and Butcher, S. E. (2009) Selection and characterization of small molecules that bind the HIV-1 frameshift site RNA. *ACS Chem. Biol. 4*, 844−854.
(28) Tanious, F. A., Veal, J. M., Buczak, H., Ratmeyer, L. S., and Wilson, W. D. (1992) DAPI (4′,6-diamidino-2-phenylindole) binds differently to DNA and RNA: minor-groove binding at AT sites and intercalation at AU sites. *Biochemistry 31*, 3103−3112.
(29) Trotta, E., D'Ambrosio, E., Ravagnan, G., and Paci, M. (1995) Evidence for DAPI intercalation in CG sites of DNA oligomer $[d(CGACGTCG)]_2$: a ^1H NMR study. *Nucleic Acids Res. 23*, 1333−1340.
(30) Trotta, E., and Paci, M. (1998) Solution structure of DAPI selectively bound in the minor groove of a DNA T.T mismatch-containing site: NMR and molecular dynamics studies. *Nucleic Acids Res. 26*, 4706−4713.
(31) Disney, M. D., Childs, J. L., and Turner, D. H. (2004) Hoechst 33258 selectively inhibits group I intron self-splicing by affecting RNA folding. *ChemBioChem 5*, 1647−1652.
(32) Miletti, K. E., and Leibowitz, M. J. (2000) Pentamidine inhibition of group I intron splicing in *Candida albicans* correlates with growth inhibition. *Antimicrob. Agents Chemother. 44*, 958−966.
(33) Childs-Disney, J. L., Wu, M., Pushechnikov, A., Aminova, O., and Disney, M. D. (2007) A small molecule microarray platform to select RNA internal loop-ligand interactions. *ACS Chem. Biol. 2*, 745−754.
(34) Disney, M. D., and Childs-Disney, J. L. (2007) Using selection to identify and chemical microarray to study the RNA internal loops recognized by 6′-N-acylated kanamycin A. *ChemBioChem 8*, 649−656.
(35) Bevilacqua, J. M., and Bevilacqua, P. C. (1998) Thermodynamic analysis of an RNA combinatorial library contained in a short hairpin. *Biochemistry 37*, 15877−15884.
(36) Serra, M. J., and Turner, D. H. (1995) Predicting thermodynamic properties of RNA. *Methods Enzymol. 259*, 242−261.
(37) Caskey, C. T., Pizzuti, A., Fu, Y. H., Fenwick, R. G. Jr., and Nelson, D. L. (1992) Triplet repeat mutations in human disease. *Science 256*, 784−789.
(38) Dervan, P. B. (2001) Molecular recognition of DNA by small molecules. *Bioorg. Med. Chem. 9*, 2215−2235.
(39) Arambula, J. F., Ramisetty, S. R., Baranger, A. M., and Zimmerman, S. C. (2009) A simple ligand that selectively targets CUG trinucleotide repeats and inhibits MBNL protein binding. *Proc. Natl. Acad. Sci. U.S.A. 106*, 16068−16073.
(40) Mills, J. E., and Dean, P. M. (1996) Three-dimensional hydrogen-bond geometry and probability information from a crystal survey. *J. Comput. Aided Mol. Des. 10*, 607−622.
(41) Grant, J. A., Gallardo, M. A., and Pickup, B. T. (1996) A fast method of molecular shape comparison. A simple application of a Gaussian description of molecular shape. *J. Comput. Chem. 17*, 1653−1666.
(42) Haigh, J. A., Pickup, B. T., Grant, J. A., and Nicholls, A. (2005) Small molecule shape-fingerprints. *J. Chem. Inf. Model. 45*, 673−684.
(43) Kanadia, R. N., Johnstone, K. A., Mankodi, A., Lungu, C., Thornton, C. A., Esson, D., Timmers, A. M., Hauswirth, W. W., and Swanson, M. S. (2003) A muscleblind knockout model for myotonic dystrophy. *Science 302*, 1978−1980.
(44) Mankodi, A., Logigian, E., Callahan, L., McClain, C., White, R., Henderson, D., Krym, M., and Thornton, C. A. (2000) Myotonic

dystrophy in transgenic mice expressing an expanded CUG repeat. *Science 289*, 1769−1773.
(45) Day, J. W., and Ranum, L. P. (2005) RNA pathogenesis of the myotonic dystrophies. *Neuromuscular Disord. 15*, 5−16.
(46) Li, L. B., and Bonini, N. M. (2010) Roles of trinucleotide-repeat RNA in neurological disease and degeneration. *Trends Neurosci. 33*, 292−298.
(47) Wojciechowska, M., and Krzyzosiak, W. J. (2011) Cellular toxicity of expanded RNA repeats: focus on RNA foci. *Hum. Mol. Genet.*,in press.
(48) Shieh, S. Y., and Bonini, N. M. (2011) Genes and pathways affected by CAG-repeat RNA-based toxicity in *Drosophila*. *Hum. Mol. Genet. 20*, 4810−4821.
(49) Tsoi, H., Lau, C. K., Lau, K. F., and Chan, H. Y. (2011) Perturbation of U2AF65/NXF1-mediated RNA nuclear export enhances RNA toxicity in polyQ diseases. *Hum. Mol. Genet. 20*, 3787−3797.
(50) Ho, T. H., Savkur, R. S., Poulos, M. G., Mancini, M. A., Swanson, M. S., and Cooper, T. A. (2005) Colocalization of muscleblind with RNA foci is separable from mis-regulation of alternative splicing in myotonic dystrophy. *J. Cell Sci. 118*, 2923−2933.
(51) Hsu, R. J., Hsiao, K. M., Lin, M. J., Li, C. Y., Wang, L. C., Chen, L. K., and Pan, H. (2011) Long tract of untranslated CAG repeats is deleterious in transgenic mice. *PLoS One 6*, e16417.
(52) Wang, L. C., Chen, K. Y., Pan, H., Wu, C. C., Chen, P. H., Liao, Y. T., Li, C., Huang, M. L., and Hsiao, K. M. (2011) Muscleblind participates in RNA toxicity of expanded CAG and CUG repeats in *Caenorhabditis elegans*. *Cell. Mol. Life Sci. 68*, 1255−1267.
(53) Li, L. B., Yu, Z., Teng, X., and Bonini, N. M. (2008) RNA toxicity is a component of ataxin-3 degeneration in Drosophila. *Nature 453*, 1107−1111.
(54) Warf, M. B., Nakamori, M., Matthys, C. M., Thornton, C. A., and Berglund, J. A. (2009) Pentamidine reverses the splicing defects associated with myotonic dystrophy. *Proc. Natl. Acad. Sci. U.S.A. 106*, 18551−18556.
(55) Fardaei, M., Rogers, M. T., Thorpe, H. M., Larkin, K., Hamshere, M. G., Harper, P. S., and Brook, J. D. (2002) Three proteins, MBNL, MBLL and MBXL, co-localize *in vivo* with nuclear foci of expanded-repeat transcripts in DM1 and DM2 cells. *Hum. Mol. Genet. 11*, 805−814.
(56) Jiang, H., Mankodi, A., Swanson, M. S., Moxley, R. T., and Thornton, C. A. (2004) Myotonic dystrophy type 1 is associated with nuclear foci of mutant RNA, sequestration of muscleblind proteins and deregulated alternative splicing in neurons. *Hum. Mol. Genet. 13*, 3079−3088.
(57) Mankodi, A., Urbinati, C. R., Yuan, Q. P., Moxley, R. T., Sansone, V., Krym, M., Henderson, D., Schalling, M., Swanson, M. S., and Thornton, C. A. (2001) Muscleblind localizes to nuclear foci of aberrant RNA in myotonic dystrophy types 1 and 2. *Hum. Mol. Genet. 10*, 2165−2170.
(58) Miller, J. W., Urbinati, C. R., Teng-Umnuay, P., Stenberg, M. G., Byrne, B. J., Thornton, C. A., and Swanson, M. S. (2000) Recruitment of human muscleblind proteins to (CUG)(n) expansions associated with myotonic dystrophy. *EMBO J. 19*, 4439−4448.
(59) Taneja, K. L., McCurrach, M., Schalling, M., Housman, D., and Singer, R. H. (1995) Foci of trinucleotide repeat transcripts in nuclei of myotonic dystrophy cells and tissues. *J. Cell. Biol. 128*, 995−1002.
(60) Gomes-Pereira, M., Cooper, T. T., and Gourdon, G. (2011) Myotonic Dystrophy mouse models: towards rational therapy development. *Trends in Mol. Med. 17*, 506−17.
(61) Childs-Disney, J. L., Tsitovich, P. B., and Disney, M. D. (2011) Using modularly assembled ligands to bind RNA internal loops separated by different distances. *ChemBioChem 12*, 2143−2146.
(62) Yu, Z., Wang, A. M., Robins, D. M., and Lieberman, A. P. (2009) Altered RNA splicing contributes to skeletal muscle pathology in Kennedy disease knock-in mice. *Dis. Models Mech. 2*, 500−507.
(63) Peyret, N., Seneviratne, P. A., Allawi, H. T., and SantaLucia, J. Jr. (1999) Nearest-neighbor thermodynamics and NMR of DNA sequences with internal A.A, C.C, G.G, and T.T mismatches. *Biochemistry 38*, 3468−3477.
(64) SantaLucia, J. Jr. (1998) A unified view of polymer, dumbbell, and oligonucleotide DNA nearest-neighbor thermodynamics. *Proc. Natl. Acad. Sci. U.S.A. 95*, 1460−1465.
(65) Puglisi, J. D., and Tinoco, I. Jr. (1989) Absorbance melting curves of RNA. *Methods Enzymol. 180*, 304−325.